Greenland annual accumulation along the EGIG line, 1959–2004, from ASIRAS airborne radar and neutron-probe density measurements

T. B. Overly[1], R. L. Hawley[1], V. Helm[3], E. M. Morris[2], and R. N. Chaudhary[1]

[1]Dartmouth College, Hanover, NH, USA
[2]Scott Polar Research Institute, Cambridge, UK
[3]Alfred Wegener Institute, Bremerhaven, Germany

Correspondence to: T. B. Overly (thomas.b.overly@dartmouth.edu)

Per the Cryosphere File Upload Instructions: "Please include a point-by-point response to the reviews, a list of all relevant changes made in the manuscript, and a marked-up manuscript version (combined in one *.pdf file)."

Point-by-Point Response to Reviews:

- See Author replies at http://www.the-cryosphere-discuss.net/tc-2015-164/discussion

Relevant Changes and Additional Responses:

- Shortened Title
- Detailed proofreading per Catania Review, resulting in major reduction in text and captions.
- Included comparisons to two additional Regional Climate Models, MAR and RACMO2.3. This change propagates throughout the document and addresses Anonymous Reviewer # 1's suggestion to include and emphasize additional models and comparisons.
- Added description of model grids and how accumulation comparisons made between ASIRAS-NP and RCM's
- Small changes to Figure 1, additional topo line label, fixed symbology, added T43 Crete
- Simplification and expansion of Figure 3.
- Removal of Appendix Table A3.
- Expansion of Tables 1 and 2 and A1 and A2. This addresses repeat comments about uncertainty/error estimates per Koenig review.
- Added Table 3 Summary of percent difference between ASIRAS-NP and Regional Climate Models
- Changes to Figure 4: Inclusion of Regional Climate Models MAR and RACMO. Point locations of grid cells rather than continuous lines. Elevation line added per reviewer suggestion

– Added references to Simonsen, Helm, Wessel, Medley, Noel, Renaud, Meige, Spikes, Arcone per reviewers suggestions and author's changes

Abstract.

We report annual snow accumulation rates from 1959 to 2004 along a 250 km segment of the Expéditions Glaciologiques Internationales au Groenland (EGIG) line across central Greenland using Airborne SAR/Interferometric Radar Altimeter System (ASIRAS) radar layers and ~~detailed~~ high resolution neutron-probe (NP) density profiles. ASIRAS-NP derived accumulation rates are not statistically different (95 % confidence interval) from in situ EGIG accumulation measurements from 1985 to 2004. Below 3000 m elevation, ASIRAS-NP derived accumulation increases by 20 % for the period 1995 to 2004 compared to 1985 to 1994. Above 3000 m elevation, accumulation increases by 13 % for 1995–2004 compared to 1985–1994. Three Regional Climate Models (PolarMM5, RACMO2.3, MAR) underestimate snow accumulation below 3000 m by 16–20 % compared to ASIRAS-NP from 1985 to 2004. We test radar-derived accumulation rates sensitivity to density using modelled density profiles in place of ~~detailed NP data~~NP densities. ASIRAS radar layers combined with Herron and Langway (1980) model density profiles (ASIRAS-HL) produce accumulation rates within 3.5 % of ASIRAS-NP estimates. We suggest using Herron and Langway (1980) density profiles to calibrate radar layers detected in dry snow regions of ice sheets lacking detailed in situ density measurements, such as those observed by the Operation IceBridge campaign.

1 ~~Introduction~~

~~An understanding of~~

1 Introduction

Estimating ice sheet mass balance requires knowledge of the gains and losses to the system. The IPCC estimates a 0.40 ± 0.15 m sea-level rise by the year 2100 (scenario RCP2.6 IPCC, 2014). Assumptions in assessing snow accumulation (the primary positive input to ice sheets) account for a portion of the uncertainty in potential sea-level rise. Studies using ice cores (Anklin and Stauffer, 1994; Bales et al., 2001, 2009; Banta and McConnell, 2007; McConnell et al., 2001; Mosley-Thompson et al., 2001) provide records of past accumulation, while climate models (Box et al., 2004; Bromwich et al., 2001; Burgess et al., 2010; McConnell et al., 2000) reconstruct accumulation in regions lacking in situ measurements. Regional Climate Models (RCMs) provide widespread spatial coverage of recent annual snow accumulation (1958–2015), but these estimates interpolate between ground-truthed point locations (Burgess et al., 2010; Noël et al., 2015; Tedesco et al., 2015). The simplification of accumulation rates from point-based measurements may be overcome using ice-penetrating radar. Radar stratigraphy studies (Arcone et al., 2004, 2005; Eisen et al., 2008; Hawley et al., 2006, 2014; de la Pena et al., 2010; Spikes et al., 2004; Medley et al., 2013, 2014) measure snow accumulation by combining in situ measurements (snow density, ice core chemistry) with continuous isochronal layers within the dry-snow zone of ice sheets. The depth of a given radar layer depends on the density of the snowpack through which the radar signal travels. ~~Accounting for density to identify~~ Using density to calculate the depth and

age of these layers allows for the estimation of an accumulation rate. Given this density and signal propagation relationship, we assume that the most accurate snow accumulation rates result from radar surveys collected simultaneously with in situ density measurements.

The European Space Agency's 2006 Airborne SAR/Interferometric Radar Altimeter System (ASIRAS) campaign detected annual accumulation layers along the Expéditions Glaciologiques Internationales au Groenland (EGIG) traverse across central Greenland (Hawley et al., 2006; de la Pena et al., 2010). Previous accumulation estimates using ASIRAS layers along EGIG incorporate a maximum of two density profiles to ~~correct~~ calculate ASIRAS travel-time (and thus determine ASIRAS layer depth) (Hawley et al., 2006; de la Pena et al., 2010). Concurrent to the 2006 radar campaign, Morris and Wingham (2011) conducted detailed measurements of near-surface density to 13 m depth using a~~Neutron Probe~~ neutron-probe (NP). Eight NP sites along a 250 km segment of the EGIG route provide ground-truthed density measurements for ~~correcting~~ calculating ASIRAS travel-time through the ice sheet's surface (~~Figure ??~~Fig. 6). We present annual accumulation rates from 1959 to 2004 derived from NP density adjusted ASIRAS layers (ASIRAS-NP accumulation record). We compare our ASIRAS-NP accumulation record to previous measurements of annual accumulation from shallow cores (Anklin and Stauffer, 1994; Fischer et al., 1995) and three Regional Climate Models (RCMs). Detailed density, collected in ~~concert~~ conjunction with an airborne radar survey, offers the opportunity to understand radar-derived accumulation rates' sensitivity to density. We test the ASIRAS accumulation rate's sensitivity to density using simple Herron and Langway modeled density profiles in place of ~~detailed~~ NP density measurements (ASIRAS-HL). Modeled density combined with radar layers may offer ~~a compromise~~ an alternative for deriving accumulation rates from radar layers lacking ~~detailed~~ ground-truthed density.

2 Background

2.1 EGIG ~~Line~~line

Major joint European expeditions across central Greenland were conducted in 1958-59 (EGIG1) and 1967-68 (EGIG2) (Renaud et al., 1963; Merlivat et al., 1973). Shallow cores drilled along the route led to the first isotopic climate curves produced by Willi Dansgaard (Dansgaard, 2004). Merlivat et al. (1973) report a tritium based mean annual accumulation from 1959–1969 of 0.329 meters water equivalent accumulation per year ($\mathrm{m\ w.e.a^{-1}}$) at site ~~T-31~~ T31 (Station Centrale) and 0.243 ($\mathrm{m\ w.e.a^{-1}}$) at site ~~T-43~~ T43 (Crête). Benson (1962) found mean annual accumulation from 1946–1955 of 0.355 ($\mathrm{m\ w.e.a^{-1}}$) at ~~T-31~~T31.

A 1990–1992 reconstruction of the EGIG line by Technische Universität Braunschweig led to glacio-meteorological, isotopic/chemical, and snow accumulation studies (Anklin and Stauffer, 1994; Fischer et al., 1995). These studies ~~revealed around 0.45 ()~~ found accumulation rates between 0.47–0.44 $\mathrm{m\,w.e.\,a^{-1}}$ at the western portion of EGIG, decreasing to ~~around~~ 0.25 to 0.20 ($\mathrm{m\,w.e.\,a^{-1}}$) along the eastern ~~interior of the ice sheet. Fischer et al. (1995) found~~ edge of the EGIG line. Fischer et al. (1995) report no long-term temporal changes in accumulation rates from 1955 to 1995.

Site ~~t21~~ T21 marks the approximate transition to the dry snow zone, with air temperatures upslope from ~~t21~~ T21 rarely exceeding 0~~°C~~ °C (Fig. 6) (Morris and Wingham, 2011). Morris and Wingham (2011) observed a transition in surface

conditions approximately 10 km uphill from site ~~t31~~T31. Elevations upslope from ~~t31~~ T31 experience less persistent winds, leaving a smooth surface with undisturbed summer surface hoar (Morris and Wingham, 2011). Down-slope from ~~t31~~ T31 the upper snow layer appears wind-packed, with sastrugi marking the surface (Morris and Wingham, 2011).

~~Detailed analysis of snow accumulation builds upon previous accumulation studies using ice cores (Anklin and Stauffer, 1994; Bales et al., 2001, 2009; Banta and McConnell, 2007; McConnell et al., 2001; Mosley-Thompson et al., 2001) models (Box et al., 2004; Bromwich et al., 2001; Burgess et al., 2010; McConnell et al., 2000) , and radar stratigraphy (Arcone et al., 2004, 2005; Eisen et al., 2008; Hawley et al., 2006; de la Pena et al., 2010; Spikes et al., 2004; Medley et al., 2013, 2014) t measure and model accumulation variability.~~

2.2 ASIRAS ~~Radar~~radar

The European Space Agency originally designed ~~the Airborne Synthetic aperture Interferometric Radar Altimetry System (ASIRAS)~~ ASIRAS to serve as a prototype for the CryoSat Mission (Stenseng et al., 2007). ASIRAS uses a Ku-band radar altimeter to measure ice sheet surface elevation and detect sub-surfaces layers. Stenseng et al. (2007) described the internal reflection horizons observed by ASIRAS as corresponding to density interfaces. ASIRAS radar has a carrier frequency of ~~13.5GHz~~ 13.5 GHz and instrument bandwidth ~~$B = 1GHz$~~ $B = 1$ GHz. The radar transect discussed in this paper was collected using Low Altitude Mode (LAM). ASIRAS-LAM has ~~$N_s = 4096$~~ $N_\mathrm{s} = 4096$ echo samples, an uncompressed pulse length of ~~$T_{uc} = 80$~~ $T_\mathrm{uc} = 80$ µs, an instrument sampling frequency of ~~$F_s = 37.5MHz$~~ $F_\mathrm{s} = 37.5$ MHz, resulting in a range bin resolution of $\Delta R = 0.109$ m, using the range-resolution equation from ~~(?) :~~

(Cullen, 2010) :

$$\Delta R = \frac{T_\mathrm{uc} F_\mathrm{s} c}{2 B N_\mathrm{s}} \tag{1}$$

where c is the speed of light, $\sim 299\,792\,458\,\mathrm{m\,s^{-1}}$.

Hawley et al. (2006) measured annual accumulation from 1995 to 2002 at site ~~t21~~ T21 using ASIRAS radar. The study used a single NP density profile, ~~t21~~T21, to calculate radar travel-time through snowpack and depth to the sub-surface layers. Hawley et al. (2006) ~~establishes ASIRAS 's~~ establish ASIRAS internal reflection horizons as annual accumulation layers, correlating high density winter peaks with local peaks in radar power return. ASIRAS accumulation layers, examined down to ~~10m~~ 10 m depth, produced a mean annual accumulation of 0.47~~m w.e. a^{-1}~~ m w.e. a^{-1} (similar to ~~Anklin and Stauffer (1994) and Fischer et al. (1995)~~ Anklin and Stauffer, 1994; Fischer et al., 1995). Hawley et al. (2006) found decreasing accumulation with increasing elevation and short-scale variability in line with ~~Fischer et al. (1995); Box et al. (2004)~~ Fischer et al. (1995) and Box et al. (2004) . Hawley et al. (2006) observe upward curved reflectors in areas of steep slope and accumulation-driven layering, in agreement with Black and Budd (1964).

Helm et al. (2007) collected simultaneous ground-based density measurements and ASIRAS overflights in the percolation zone along EGIG (downslope from this study). The dominant second peak observed in the ASIRAS waveform results from a heterogeneous zone of metamorphosed snow and ice lenses below the winter snowpack (Helm et al., 2007). From this finding, Helm et al. (2007) demonstrate ASIRAS's ability to derive winter accumulation rates. Similar to Black and Budd (1964);

Hawley et al. (2006), Helm et al. (2007) found a strong correlation between surface gradient and accumulation rate, with higher accumulation rate in the plateau areas and lower accumulation rate on slopes.

de la Pena et al. (2010) presented mean accumulation rates for the period 1998–2003, calculated from six ASIRAS internal reflection horizons layers along 200 km of the EGIG route. de la Pena et al. (2010) used the published t21 published T21 NP density values from Hawley et al. (2006) and a Summit density profile (located 150 km north of the EGIG line) to linearly interpolate density values, calculate radar travel-time through snow/firn layers, calculate layer depth and accumulation rates along the EGIG routeline. de la Pena et al. (2010) report an average accumulation of 0.36m w.e. a^{-1} m w.e. a^{-1} with high spatial and temporal variability, and aclear decreasing accumulation gradient from west to east along the EGIG line. The observed accumulation gradient is EGIG consistent with previous studies of Anklin and Stauffer (1994); Fischer et al. (1995) , Anklin and Stauffer (1994) , Fischer et al. (1995) , Burgess et al. (2010) , and the interannual variability observed by (Fischer et al., 1995) Fischer et al. (1995) . de la Pena et al. (2010) presented a 15–20 % increase in accumulation above 3000m 3000 m over the past 20-25yrs 20–25 yrs compared to Anklin and Stauffer (1994).

Simonsen et al. (2013) use ASIRAS layers down to approximately 15 m depth along EGIG to assess firn compaction. They use an automatic method to identify ASIRAS layers and confirm the layers represent isochrones spaced 1 year apart (Simonsen et al., 2013). Accumulation rates are not reported, as the study focused on firn compaction.

2.3 EGIG-Ground In-Situ Measurementsin situ measurements

2.3.1 Shallow Core Accumulationcore accumulation

Anklin and Stauffer (1994) drilled eleven shallow firn cores (referred to as t-sitesT-sites, Fig. ??6), 8 to 10 m depth, about every spaced 50 km apart along the EGIG line. Using hydrogen peroxide (H_2O_2 H_2O_2) analysis and snow density to identify the seasonal signal, Anklin and Stauffer (1994) report annual accumulation from 1969 to 1989 for t-sites T-sites along the EGIG line(0.44 $^{-1}$ along the western portion, 0.25 $^{-1}$ at the eastern margin). Their accumulation rates fit with the general understanding of water vapor transport and snow accumulation across the Greenland Ice Sheet; higher accumulations along the coast : higher accumulations near the coast (0.44 m w.ea^{-1}) gradually decreasing with increasing elevation (0.25 m w.ea^{-1} at the east end of EGIG). Anklin and Stauffer (1994) found large variations of local annual accumulation rates from 1979 to 1989, with typical standard deviations of 10 to 25 %. Changes in annual accumulation correlated from site to site. Temporally, annual accumulation increased slightly in central Greenland and decreased slightly at middle and low elevations.

Fischer et al. (1995) drilled eighteen shallow firn cores along the EGIG line during field campaigns in 1990 and 1992. Annual accumulation rates from 1984–1989 were determined by counting seasonally varying tracers $\delta^{18}O$ $\delta^{18}O$ and major ions. Measurements were collected at approximately eight samples per year. The 1990 campaign used seasonally varying hydrogen peroxide (H_2O_2 H_2O_2) analysis (in collaboration with Anklin and Stauffer (1994) Anklin and Stauffer, 1994) to determine summer maxima of flourimetric profiles. Fischer et al. (1995) observed distinct winter/summer pairings in the upper snow. Fischer et al. (1995) found layer thickness and accumulations similar to Anklin and Stauffer (1994) , with highest (0.47–0.43 m w.e. a^{-1}), along the western portion of EGIG (0.47 to 0.43 $^{-1}$), decreasing to the east (0.25 to 0.20^{-1} m w.e. a^{-1},

though fewer measurements exist to support the eastern accumulation rates). Fischer et al. (1995) argues for accumulation variations along EGIG due to large scale topographic valleys and ridges. The short timespan of the study, 1984 to 1989, limited the identifiable temporal trend (Fischer et al., 1995).

2.3.2 ~~Neutron Probe Densities~~ Neutron-probe densities and ~~Accumulation~~accumulation

Morris and Wingham (2011) collected near-surface ~~in-situ neutron probe~~ in situ neutron-probe (NP) density measurements along a 365 km section of the EGIG line in the Spring and Autumn of 2004 and Spring and Summer of 2006 (Morris and Wingham, 2014). The 2006 traverse coincided with airborne observations of sub-surface layers using ASIRAS. The probe used by Morris and Wingham (2011) consists of an annular radioactive americium-241/beryllium source of fast neutrons around a cylindrical detector of slow (thermal) neutrons (Morris and Cooper, 2003). The fast neutrons lose energy by scattering as they move through the snow. The count rate of slow neutrons arriving back at the detector per unit time relates to the density of the snow (Morris and Wingham, 2011). Morris (2008) derived theoretical calibration equations for count rate and snow density. ~~Descriptions of the neutron probe data collectioncan be found in Morris and Wingham (2011, 2014)~~ See Morris and Wingham (2011) , Morris and Wingham (2014) for descriptions of NP data collection.

~~The traverses span ice-sheet elevations of 1940 to 3201, with accumulation generally decreasing with increasing elevation.~~ Morris and Wingham (2011) collected seventeen "~~t-site~~T-site" NP density profiles and accumulation rates spanning ice-sheet elevations of 1940 to 3201 m, (eight NP ~~t-sites~~ T-sites of this study mapped on ~~Figure ??~~Fig. 6). The NP measured snow density from the surface down to approximately ~~13m~~ 13 m depth at the ~~t-sites~~ T-sites along the EGIG traverse. ~~Density fluctuates between high-density winter peaks and low-density summer troughs (see Morris and Wingham (2011)). The vertical distance between successive winter density peaks defines a NP annual layer (Hawley et al., 2008) . Morris and Wingham (2011)~~ Morris and Wingham (2011) observe that the density peaks lie in winter snow and are formed during the following summer when warm temperatures promote densification in the near surface layers. This transition in snow density marks the annual seasonal change detected by ASIRAS (Hawley et al., 2006; de la Pena et al., 2010). The snow thickness between density peaks, adjusted to mean water-equivalent using density measurements, ~~provides an~~ defines the NP estimate of annual accumulation (Hawley et al., 2008; Morris and Wingham, 2011).

3 Methods

3.1 ASIRAS traced layers

We focus on a 250 km segment of the EGIG line spanning eight NP ~~t-sites (Figure ??~~T-sites (Fig. 6). We trace ~~thirty~~ 48 layers down to ~~20m~~ 20 m depth from a 29 April 2006 ASIRAS flight radargram (~~Figure ??~~Fig. 2). Our radar profile starts ~~with~~ at T21a (0 km distance~~at the site of t21a at 2700m~~) 2700 m elevation and ends 250 km to the east beyond the ice divide ~~below 3200m. The radargram has been processed from~~ (3200 m elevation). Using SAR processed level SUBSCRIPTNB~~1b ASIRAS datausing~~ 1b ASIRAS data, we apply the following signal processing techniques: waveform

alignment, stacking, and gain. Each column of the radargram represents the centered mean of the surrounding 100 columns (hence 100 columns "stacked" into one record, representing approximately three horizontal meters). The ASIRAS signal weakens with increasing depth through the snowpack, thus we apply a ramped gain to the signal to enhance the visual contrast of the radargram. The ramped gain resembles an exponential gain, resulting in a 3× enhancement of layer intensity at ~~15m~~ 15 m depth and an 8~~enhancement at 20m depth. Deeper layers appear faint near the western portion of EGIG (0 to 75) where seasonal melt in the upper layers attenuates the radar signal.~~ × enhancement at 20 m depth.

We trace layers by tracking the maximum reflected power. The trace progresses by searching the adjacent column for a maximum power reflected within the vertical range of a moving window. Automated layer tracing occurs one layer at a time with visual inspection and user approval of the final traced layer. The shallowest (1st) layer represents the 2005 accumulation surface and the deepest (48th) traced layer represents the 1959 accumulation year (~~Autumn~~ October 1958 to ~~Autumn~~ September 1959) ~~. The deeper layers~~ (Fig. A1). Layers fade in intensity around 16 m depth along the western section of ~~the line (0-75~~ EGIG (0–75 km) and ~~also with increasing~~ at 14 m depth along the rest of the line (~~75–250~~ 75–250 km). The exact depth depends on the ASIRAS electromagnetic wave speed v (~~m s^{-1}~~ m s^{-1}) through the snowpack. Electromagnetic wave speed ~~v~~ v relates to the real part of the dielectric permittivity ~~ϵ_r~~ ϵ_r (dimensionless) which in the near-surface can be related to density ρ (~~kg m^{-3}~~ kg m^{-3}) by (~~Kovacs et al. (1995)):~~

Kovacs et al., 1995):

$$v = \frac{c}{\sqrt{\epsilon_\mathrm{r}}} \tag{2}$$

$$\epsilon_\mathrm{r} = (1 + 8.45 \times 10^{-4} \rho)^2 \tag{3}$$

where c is the speed of light in a vacuum ($\sim 299\,792\,458$ m s^{-1}).

Signal travel-time will change based on the density of the snowpack. Dense coastal snowpack slows the signal speed compared to a less dense interior snowpack. Near the coast 45 nanoseconds (ns) of travel-time equals 5.10~~m~~ m depth while the same travel-time in the interior would equal 5.15 m depth. ASIRAS corrected with a coastal density profile gives a depth of 20.03~~m at 190ns~~ m at 190 ns. The same ~~190ns~~ 190 ns travel-time reaches 20.24~~m~~ m depth using the interior NP profile. The near-surface difference in travel-time being unresolvable given ASIRAS's 0.109 m range-bin resolution (Section 2.2).

All ASIRAS-derived accumulation rates have the same radar-time ~~positions of layers~~layer positions. The density used to adjust the radar signal propagation determines the depth, and therefore thickness of an annual accumulation layer. ASIRAS-NP~~accumulation rate discussed in Section ??~~ , discussed in Sect. 3.3.1, interpolates densities between eight NP density profiles (~~Section~~ Sect. 3.2) to calculate layer depths. ASIRAS-HL~~discussed in Section ??~~ , discussed in Sect. 3.2.2, uses ASIRAS layers with HL density profiles to calculate layer depths.

3.2 Density profiles

3.2.1 ~~Neutron Probe Density~~

3.2.1 Neutron-probe density

Detailed density profiles allow for more accurate calculations of ASIRAS radar-travel-time through the snowpack. Previous studies along EGIG (de la Pena et al., 2010; Hawley et al., 2006) rely on a maximum of two density profiles to constrain radar travel-time for determination of layer depth. We expand the range of ground-truthed NP density measurements by combining sixteen previously published ~~density profiles (Morris and Wingham, 2011)~~ (Morris and Wingham, 2011) density profiles from eight T-sites (~~t21a, t23, t27, t31, t35, t39, t41~~T21a, T23, T27, T31, T35, T39, T41) in the dry-snow zone above ~~2700m (Figure ??~~2700 m (Fig. 2). The deepest NP measurements are ~~11m~~11 m, while our deepest ASIRAS layer reaches ~~21m depth. Below 11m depth, we estimate densities~~ 30 m depth. We calculate densities below 11 m using the centimeter resolution density ~~50m~~ GISP2 B-core (NSIDC, 1997) at Summit. The easternmost NP density measurement (~~t41) at 10m~~ T41) at 10 m depth (0.538~~g m^{-3}~~ g m^{-3}) is similar to the GISP2 B-core density value at ~~10m~~ 10 m core depth (0.529~~g m^{-3}). We use GISP2 B-core "Shifted" densities to correct radar travel-time from the deepest NP measurement to the deepest ASIRAS layer.~~ g m^{-3}). The western edge of EGIG, at ~~2700m~~ 2700 m elevation, has a~~10m~~ 10 m density of 0.559~~g m^{-3}~~ g m^{-3}. We assume ~~the rate~~ similar rates of densification below ~~10m depth is similar at t21a, t41~~10 m depth at T21a, T41, and GISP2. We ~~shift~~ append the GISP2 profile at ~~10m~~ 10 m depth to start where ~~t21a~~ T21a NP density profile ends.

3.2.2 Herron and Langway model density

3.2.3 ~~Herron and Langway Model Density~~

Logistical challenges for both ice coring and NP logging ~~spatially limit~~ limit spatially detailed density measurements. Herron and Langway (1980)'s simple empirical model of polar snow densification provides an alternative for estimating ice sheet density in the absence of ~~in-situ~~ in situ measurements. The model allows us to generate a density profile at any point along EGIG with three input parameters: mean annual accumulation ~~A~~ A, mean annual temperature ~~T~~ T, and initial surface snow density ~~ρ_0~~ ρ_0. The model has two stages of densification for depths above and below the "critical density" $\rho = 0.55\,\mathrm{Mg\,m^{-3}}$. The "critical density" marks the transition from first-stage rapid densification due to grain settling and packing to second-stage slowed densification with depth (Herron and Langway, 1980). The model equations used for density ρ at depth ~~h~~ h for the two

stages of densification:

Pre-critical:

$$\rho_h = \frac{\rho_i \zeta_0}{1+\zeta_0}$$

$$\zeta_0 = \exp\left[\rho_i k_0 h + \ln\left(\frac{\rho_0}{\rho_i - \rho_0}\right)\right]$$

$$k_0 = 11 \cdot \exp\left(\frac{-10160}{R \cdot T}\right)$$

Post-critical:

$$\rho_h = \frac{\rho_i \zeta_1}{1+\zeta_1}$$

$$\zeta_1 = \exp\left[\rho_i k_1 \frac{(h - h_{0.55})}{A^{0.5}} + \ln\left(\frac{0.55}{\rho_i - 0.55}\right)\right]$$

$$k_1 = 575 \cdot \exp\left(\frac{-21400}{R \cdot T}\right)$$

~~where k_0 and k_1 are Arrhenius-type rate constants, gas constant $R = 8.314$, $T =$ temperature in kelvin, $h_{0.55} = \frac{1}{\rho_i k_0}[ln\frac{0.55}{\rho_i - 0.55} - \frac{\rho_0}{\rho_i - \rho_0}]$ with the density of ice $\rho_i = 0.917$.~~ where $h_{0.55} = \frac{1}{\rho_i k_0}[\ln\frac{0.55}{\rho_i - 0.55} - \frac{\rho_0}{\rho_i - \rho_0}]$, k_0 and k_1 are Arrhenius-type rate constants, and gas constant $R = 8.314\,\mathrm{J\,K^{-1}\,mol^{-1}}$, $T =$ temperature

We calculate densities along EGIG using mean annual accumulation from Burgess et al. (2010), temperatures from Steffen and Box (2001), and Morris and Wingham (2011)'s ~~t-site~~ T-site surface densities as inputs to Herron and Langway (1980)'s model. We use densities generated from Herron and Langway (1980)'s model to adjust radar travel-time and derive the ASIRAS-HL accumulation rate as a comparison to the NP derived ASIRAS-NP accumulation rates.

3.3 Accumulation ~~Rates~~ rates from ASIRAS

3.3.1 ASIRAS-NP: ~~Accumulation~~ accumulation rate using ~~Neutron Probe Densities~~neutron-probe densities

The sixteen NP density profiles at eight ~~t-sites (t21a, t23, t27, t31, t35, t39, t41~~T-sites (T21a, T23, T27, T31, T35, T39, T41) bound by the combined ~~t21a~~ T21a and GISP2 b-core densities on the west and the ~~t41~~ T41 and GISP2 b-core on the east, provide the anchor points for interpolating depth-density values at every point along the EGIG line. We calculate annual accumulation rates from 1959 to 2004 at the ~~t-sites (Appendix TableA1 ??~~T-sites (Table A1). We refrain from calculating a 2005 annual accumulation due to its proximity to the April 2006 ice sheet surface at time of radar and NP collection. The NP based densities represent the most detailed density measurements along EGIG~~and correct~~, correcting ASIRAS travel-time through the snowpack to create the ASIRAS-NP accumulation rates.

3.3.2 ASIRAS-HL: accumulation rate using Herron and Langway densities

3.3.3 ~~ASIRAS-HL: Accumulation rate using Herron and Langway Densities~~

Taking detailed NP density measurements remains beyond the scope of most radar surveys. We explore using simple Herron and Langway (1980) model densities (HL) to produce accumulation rates from ASIRAS radar layers (ASIRAS-HL). We examine the accumulation rate difference when using modeled density data (ASIRAS-HL) and using ~~detailed~~ NP density (ASIRAS-NP). Using spatially continuous input parameters of accumulation, temperature, and surface density, we generate HL density

profiles for ~~the 74038 radar trace locations along the 250km~~ each radar trace (one approximately every 3 m horizontally, Sect. 3.1) along the 250 km segment of EGIG.

We examine accumulation rate sensitivity to density by reducing the number of HL density profiles used to correct layer depth along the ~~250km~~ 250 km EGIG segment. Distance intervals and their corresponding number of density profiles per the 250 km EGIG segment are: 250 km (HL250, 1 profile), 125 km (HL125, 2 profiles), 50 km (HL50, 5 profiles), 30 km (HL30, 8 profiles), and 15 km (HL15, 17 profiles). We interpolate between the HL profiles to obtain a density profile at every point along EGIG.

3.4 EGIG-Ground ~~Accumulation Measurements~~accumulation measurements

We combine shallow firn core records from Anklin and Stauffer (1994) and NP based accumulation rates calculated by Morris and Wingham (2011) to establish EGIG-Ground records spanning ~~1978 to 2004 at t21, t27, t31, t41. Site t43~~ 1978–2004 at T21, T27, T31, T41. Site T43 has twelve annual accumulations from 1976 to 1988 but no NP measurements (Anklin and Stauffer, 1994). Anklin and Stauffer (1994) cores generally span 1978 to 1988 while the Morris and Wingham (2011) accumulation rates span the mid-1980's to 2004. We use the mean of the two records at site ~~t41 where the two records~~ T41 where the studies overlap. Sites ~~t21, t27, and t31~~ T21, T27, and T31 do not have overlapping records, with no accumulation rates for years 1989 and 1990 at ~~t21 and t27~~ T21 and T27 and 1989 for ~~t31~~T31. These EGIG-Ground records serve as a basis for comparison of accumulation rates derived from ASIRAS layers (~~Figure ??~~Fig. 3).

3.5 ASIRAS-NP comparison to Regional Climate Models

We validate ASIRAS-NP accumulation rates using EGIG-Ground point accumulation records (Anklin and Stauffer, 1994; Morris and Wingham, 2011) , then compare our results to accumulation rates from three Regional Climate Models (RCMs): Modèle Atmosphérique Régional (MAR)(Tedesco et al., 2015) , the polar version of the Regional Atmospheric Climate Model (RACMO2.3) (Noël et al., 2015) , and the calibrated Fifth Generation Mesoscale Model modified for polar climates (Polar MM5) (Burgess et al., 2010) .

As discussed in Sect 2.3 and Sect. 3.1, ASIRAS waveform results from a heterogeneous zone of metamorphosed snow and ice lenses below the winter snowpack (Helm et al., 2007; Morris and Wingham, 2011) . Therefore we define the ASIRAS-NP accumulation year as representing October to September. Comparisons between ASIRAS-NP and the RCMs occur by sampling ASIRAS-NP at the RCM grid points along the 250 km EGIG segment (Fig. 4). MAR annual snow accumulation spans 1958 to 2013 (Tedesco et al., 2015) . Data obtained for this study defines the accumulation year as January to December. MAR has a 25 km spatial resolution, resulting in approximately eleven MAR accumulation estimates along the 250 km EGIG line.

RACMO2.3 estimates monthly cumulated total surface mass balance (SMB) (with SMB defined as precipitation minus sublimation, snow erosion, and runoff) for the period 1958–2013 ((Noël et al., 2015)). We sum RACMO2.3 monthly accumulation values from October to September to align annual accumulation with the ASIRAS-NP defined accumulation year of (Sect. 3.1). The RACMO2.3 spatial resolution of ~11 km results in twenty-four modeled accumulations along EGIG.

Burgess et al. (2010) re-sample the Polar MM5's 24 km horizontal grid output to a 1.25 km equal-area grid using bilinear interpolation (Burgess et al., 2010; Rignot et al., 2008) . Polar MM5's hydrologic year spans September 15 to September 14. The 24 km original spacing results in approximately eleven Polar MM5 data points along the 250 km EGIG line. The Burgess et al. (2010) 1.25 km grid down sampled to our 2 km grid results in 125 points along EGIG. Using Generic Mapping Tools (GMT) (Wessel et al., 2013) `nearneighbor` command with bilinear interpolation we interpolate from the 1.24 km grid to a 2 km grid spacing.

4 Results

4.1 ASIRAS-NP ~~Accumulation Rate~~accumulation rate

The layers detected by ASIRAS ~~and adjusted with the detailed NP profiles~~provide a with depths calculated using NP profiles, provide a spatially continuous record of accumulation across 250 km of the EGIG route. We trace layers to ~~thirty-four~~ thirty meters depth and report accumulation rates for forty-six layers spanning ~~1959 to 2004 (Appendix Figure ??~~1959–2004 (Fig. A1). The mean accumulation rate for the entire ~~250km~~ 250 km EGIG segment is 0.337 m w.e. a^{-1} from 1959 to ~~2004 .~~ 2004. We focus our reported results on the period 1985 to 2004, during which EGIG-Ground measurements exist for comparison. Figure~~??~~ 2 displays spatial and temporal variations in layers across the EGIG segment.

Temporally, accumulation rates increase over time, with the onset of increase occurring in the mid-1970s. From 1959 to 1964, mean accumulation was 0.277 m w.e. a^{-1}. From 1965 to 1974, mean accumulation was 0.270 m w.e. a^{-1}. From 1975 to 1984, mean accumulation was 0.327 m w.e. a^{-1}. Mean ASIRAS-NP accumulation from 1985 to 1994 was 0.329 m w.e. a^{-1}. Accumulation for the period 1995 to 2004 (0.382 m w.e. a^{-1}) increases by 16 % compared to the previous ~~10-year~~ 10 year period. Table 1 summarizes the ~~10-year~~ 10 year mean accumulation results. ~~Please see the Appendix Table??~~ See Table A1 for detailed accumulations from 1959 to ~~1984.~~ 2004.

Spatially, accumulation decreases with increasing elevation and distance from the coast. Mean annual accumulation for 1985 to 2004 at T21a (0 km) is 0.462 m w.e. a^{-1}, gradually decreasing to 0.380 m w.e. a^{-1} at T31, 0.297 m w.e. a^{-1} at T41, and 0.254 m w.e. a^{-1} at the 250 km mark (Table A1). Using the transition in surface conditions occurring near T31 to divide EGIG, we examine accumulation rate changes over time above and below T31. Below T31, mean accumulation increased by 20 % over the 10 year period 1995 to 2004 (0.465 m w.e. a^{-1}) compared to the 1985 to 1994 period (0.387 m w.e. a^{-1}). Above T31 ~~, with undisturbed summer surface hoar from less persistent winds,~~ accumulation increased by 13 % over the 10 year period 1995 to 2004 (0.335 m a^{-1}) compared to the 1985 to 1994 period (0.296 m a^{-1}). ~~In the following sections we validate ASIRAS-NP accumulation rates by comparison to EGIG-Ground point accumulation records (Anklin and Stauffer, 1994; Morris and Wingham, 2011) and accumulation rates from three Regional Climate Models (RCMs): Polar MM5 (Burgess et al., 2010) Modle Atmosphrique Rgional (MAR)(Tedesco et al., 2015) .~~

4.2 ~~ASIRAS-NP vs. EGIG-Ground~~

4.2 ASIRAS-NP and RCMs vs. EGIG-Ground

The published EGIG-Ground ~~in-situ~~ in situ accumulation records discussed in ~~Section ??~~ Sect. 3.4 serve as the "known" accumulation rate to which we compare our ASIRAS-NP record and the RCMs. We focus on four sites (~~t21, t27, t31, t41~~T21, T27, T31, T41) that have accumulation records from both Anklin and Stauffer (1994) and Morris and Wingham (2011). ~~We also include t43 (Crete) record, which has twelve measurements from 1976 to 1988 (Anklin and Stauffer, 1994) . Figure??~~ Figure 3 presents these comparisons at the ~~five t-sites. A "box and whisker" plot of accumulation values for EGIG-Ground, ASIRAS, and Polar MM5 appear in the lower panel of Figure ??.~~ four T-sites. We compare the full records year by year using a nonparametric Wilcoxon sign-rank test designed for two populations with paired observations. The ~~test is performed on the difference of paired yearly accumulations. The ASIRAS-NP and EGIG-Ground accumulation differences have distributions whose medians are zero at sites t21, t27, t31, and t41~~differences of the paired observations will have a distribution whose median is zero at the 5 % significance level if the two populations are not statistically different. The zero median of the paired and differenced records indicate the ASIRAS-NP and EGIG-Ground accumulations come from identical populations. The paired ~~records at sites t21, t27, t31, t41, though identical, have varying strengths of similarity. Appendix Table ?? presents the probability, p, of observing a test statistic as or more extreme than the observed value. The Wilcoxon sign rank test at site t-43, with only twelve ground measurements for comparison, shows EGIG-Ground and ASIRAS-NP~~ yearly accumulations for RCMs and EGIG-Ground at the four T-sites are significantly different based on a Wilcoxon signed-rank test. In addition to the year by year comparisons, ~~we found that 1985 to 2004~~ no statistical difference exists between EGIG-Ground and ASIRAS-NP ~~accumulation rates are not statistically different at sites t21, t27, t31, t41 from Anklin and Stauffer (1994); Morris and Wingham (2011) (Table??~~mean accumulation from 1985 to 2004 at sites T21, T27, T31, T41 (Table 2). We conducted an analysis of variance test to compare means of the ~~20-year (1985-2004~~20 year (1985–2004) annual snow accumulation for ASIRAS-NP and EGIG-Ground, and the ~~Polar MM5~~ RCMs and ASIRAS-NP accumulation for 1978 to 2004. Significance differences were determined for alpha~~< 0.05. Again, EGIG-Ground and ASIRAS accumulation at site t-43 are significantly different. Comparing the yearly accumulations for the entire record,~~ < 0.05. Pearson's correlation coefficients for ASIRAS-NP and EGIG-Ground and ~~ASIRAS accumulations range from 0.75–0.16 (Appendix Table??~~RCM accumulations for the entire record (1959–2004) range from 0.56 to 0.19 (Table 6).

4.3 ASIRAS-NP vs. Regional Climate Models

~~ASIRAS-NP~~ Regional Climate Models RACMO2.3, MAR, and Polar MM5~~accumulation~~ , generally underestimate mean annual snow accumulation along EGIG compared to ASIRAS-NP (Fig. 4). ASIRAS-NP and the RCM accumulation rates from 1978 to 2004 positively correlate at ~~t-sites t-21, t-23, t-27, t-41, t-43 (Appendix Table??~~T-sites T21, T23, T27, and T41 for MAR, MM5, and RACMO2.3 (Table 6). An ANOVA comparison of means for ~~1978~~ 1959 to 2004 between ~~Polar MM5~~ shows RCM and ASIRAS-NP ~~shows~~ mean accumulations are statistically different at ~~t-sites t21, t27, t31, and t41. Polar MM5 and ASIRAS-NP accumulations at t43 are not statistically different. Using aWilcoxon sign rank test~~T-sites T21, T27, T31,

and T41. Using a Wilcoxon signed-rank test, year to year comparisons show significant statistical differences between ~~Polar MM5~~ all three RCMs and ASIRAS-NP at ~~t-sites t21, t27, t31, t41. The mean comparison excludes site t43, which lacks NP measurements. Polar MM5 mean~~ the T-sites. RCM mean accumulations along EGIG are significantly lower for the time period coincident with EGIG-Ground measurements, 1985 to 2004 (~~Figure ??~~Fig. 4). We focus on the period 1985 to 2004 to ~~derive~~ calculate standard uncertainty ($\frac{\sigma}{\sqrt{n}}$, where σ = standard deviation and ~~n=20~~$n = 20$).

Mean ~~Polar MM5 accumulation (0.293~~ RACMO accumulation (0.297 m w.e. a^{-1}) from 1985 to 2004 across the entire 250 km EGIG segment is ~~17~~18 % lower than ASIRAS-NP (~~0.355)~~ 0.356 m w.e. a^{-1}) (Table 3). Mean ASIRAS-NP and ~~Polar MM5~~ RACMO accumulations rates from 1985 to 2004 differ spatially along EGIG ~~.~~(Fig. **??**). Using the transition in surface conditions occurring near ~~t-31~~ T31 (3000 m elevation) to divide EGIG, ~~Polar MM5~~ RACMO underestimates accumulation by ~~28downslope from t-31~~ 16 % downslope from T31 compared to ASIRAS-NP. Above ~~t-31, with undisturbed summer surface hoar from less persistent winds, mean Polar MM5 accumulation is 20~~T31, mean RACMO accumulation is 18 % lower than ASIRAS-NP. Accumulation rates change over time with differing rates above and below ~~t-31.~~ T31. RACMO underestimates accumulation down-slope of T31 by 17 % compared to ASIRAS-NP from 1995 to 2004. Below T31 from 1985 to 1994 RACMO accumulation estimates are 9 % lower than ASIRAS-NP. Above T31, RACMO underestimates accumulation by 16 % for the 1985–1994 period and 17 % for 1995–2004, relative to ASIRAS-NP.

Mean MAR accumulation (0.336 m w.e. a^{-1}) from 1985 to 2004 across the entire 250 km EGIG segment is 3 % lower than ASIRAS-NP (0.355 m w.e. a^{-1}). Spatially, MAR both underestimates and overestimates accumulation along EGIG. MAR underestimates accumulation by 16 % downslope from T31 compared to ASIRAS-NP. Above T31, mean MAR accumulation rates are 4 % higher than ASIRAS-NP. Accumulation rates vary over time with differing rates above and below T31. MAR accumulations from 1995 to 2005 are ~~35higher than Polar MM5~~ 17 % lower than ASIRAS-NP accumulations down-slope of ~~t-31. Below t-31~~ T31. Below T31 from 1985 to 1994 ~~ASIRAS-NP accumulations are 21higher than Polar MM5~~MAR accumulations are 8 % lower than ASIRAS-NP. East of ~~t31, where surface conditions stabilize, ASIRAS-NP accumulation is 23~~T31, MAR accumulation is 10 % higher for 1985–1994 and 3 % higher for 1995–2004, relative to ASIRAS-NP (Table 3).

Mean Polar MM5 accumulation (0.293 m w.e. a^{-1}) from 1985 to ~~1994 and~~ 2004 across the entire 250 km EGIG segment is 17 % lower than ASIRAS-NP (0.356 m w.e. a^{-1}). Mean ASIRAS-NP and Polar MM5 accumulations rates from 1985 to 2004 differ spatially along EGIG. Using the transition in surface conditions occurring near T31 (3000 m elevation) to divide EGIG, Polar MM5 underestimates accumulation by 20 % downslope from T31 compared to ASIRAS-NP. Above T31, mean Polar MM5 accumulation is 15 % lower than ASIRAS-NP. Accumulation rates change over time with differing rates above and below T31. Polar MM5 underestimates accumulation down-slope of T31 by 16~~higher for~~ % compared to ASIRAS-NP from 1995 to ~~2004, relative~~ 2004. Below T31 from 1985 to 1994 Polar MM5 accumulation estimates are 25 % lower than ASIRAS-NP. Above T31, Polar MM5 underestimates accumulation by 12 % for the 1985–1994 period and 19 % for 1995–2004, relative to ASIRAS-NP.

4.4 ASIRAS-NP vs. ASIRAS-HL: ~~Accumulation~~ accumulation rate sensitivity to density

Mean percentage accumulation differences between ASIRAS-NP and ASIRAS-HL decrease with increasing age/depth of the layers (~~Figure~~ Fig. 5). Figure 5 plots the mean difference between ASIRAS-NP and ASIRAS-HL for the upper five (~~2000 to 2004), lower five (1985-1989~~2000–2004), period (1985–1989), and ~~1985 to 2004~~ the 20 year period 1985–2004 layers. On average the deeper the layer, the lower the difference between ASIRAS-NP and ASIRAS-HL accumulation rates. The upper five layers differ by 4 % on average. The ~~lower five layers differ~~ 1985–1989 period differs by 3.2 %. Overall, for the period ~~1985 to 2004~~1985–2004, mean ASIRAS-HL accumulation is 4.5 % lower than ASIRAS-NP accumulation.

We test sensitivity to density by limiting the number of HL density profiles along EGIG and interpolating density values between the profiles. Using one density profile (~~HL250km~~HL250 km) for the entire 250 km EGIG segment results in a 10 % difference in ASIRAS-NP and ASIRAS-HL. Incorporating two density profiles (~~HL125km~~HL125 km) halves the accumulation difference from 10 to 5 %. The ASIRAS-NP and ASIRAS-HL accumulation difference reduces to 3~~for HL50km~~ % for HL50 km (5 profiles), ~~HL30km~~ HL30 km (8 profiles), and ~~HL15km~~ HL15 km (17 profiles).

5 Discussion

5.1 ASIRAS-NP ~~Accumulation Rate~~accumulation rate

The ASIRAS layers combined with NP density data improve understanding of accumulation between ~~t-sites~~T-sites, showing detailed peaks and valleys in accumulation as seen and attributed to topography by ~~Arcone et al. (2005); Hawley et al. (2006); Black and Budd (1964); Miége and et. al. (2013)~~ Arcone et al. (2005) , Hawley et al. (2006) , Black and Budd (1964) , Miége and et. al. (2013) . The undulating layers observed in ~~Figure ??~~ Fig. 2 reinforce ice core observations of high spatial variability (Spikes et al., 2004). Spatial variability decreases with increasing depth, as layers undergo compaction. The fluctuations of layer depth and vertically aligned dips and peaks may indicate surface accumulation anomalies (Arcone et al., 2005). A gradual horizontal migration of undulations over time could produce spatially periodic accumulation rates, as described by Arcone et al. (2005). Undulations preserved from year to year are visible east of ~~t27~~ T27 at 60 km and from 125 to 175 km along the EGIG line (~~Figure ??~~Fig. 2 and Fig. A1). The oscillations are visible along the 250km EGIG segment in the long term mean temporal accumulation rate in ~~Figure ??~~ Fig. 4. Visual inspection of layer thickness for a given year (~~Figure ??~~Fig. 2 and Fig. A1) allows us to argue for high confidence in the extreme values measured by ASIRAS-NP.

In comparison to historical records, de la Pena et al. (2010) and Hawley et al. (2014) observed accumulation increases of 19 and 10 % over the last 30 and 52~~years~~ years, respectively, in high-elevation interior Greenland. We report ~~an~~ a 16 % increase in accumulation for the period ~~1995 to 2004 compared to 1985 to 1994.~~ 1995–2004 compared to 1985–1994 and a 41 % increase in accumulation for the period 1965–1974 (Table 1. We observe an east-west gradient along EGIG of increasing accumulation, with lower accumulation increases in the east and higher increases to the west. The east-west gradient strengthens

from ~~1995–2004~~1995 to 2004, when ASIRAS-NP is 20 % higher than ASIRAS-NP below ~~t-31~~ T31 and 13~~higher above t-31.~~ % higher above T31,

5.2 ASIRAS-NP vs. EGIG-Ground

The patterns observed by ~~Anklin and Stauffer (1994); Fischer et al. (1995); Morris and Wingham (2011) at the t-sites~~ Anklin and Stauffer (1994) , Fischer et al. (1995) , Morris and Wingham (2011) at the T-sites align with the overall trend observed by de la Pena et al. (2010) along EGIG of decreasing accumulation from the coast to the interior. The year-to-year comparisons from Fig~~??~~ , 3 using Paired Wilcoxon ~~rank sign~~ signed-rank span every year with observations for both ASIRAS-NP and EGIG-Ground. Year to year comparisons show that ASIRAS-NP tracks the EGIG-Ground measurements consistently. EGIG-Ground accumulation minima and maxima are not always consistent across the EGIG route for a given year (e.g. the ~~t31~~ T31 record's maxima occurs in 1995, while ~~t27 and t41~~ T27 and T41 records have near minimum values for 1995). ~~Fluctuation from~~ We attribute site to site accumulation fluctuation in the EGIG-Ground record ~~is due~~ to the limited spatially extent of a given shallow core or snowpit. Accumulation extremes seen in the ASIRAS-NP record are consistent across the ~~t-sites (low accumulation~~ T-sites (low in 1998, ~~accumulation~~ high in 1996). ~~A Wilcoxon sign rank test at site t-43 shows EGIG-Ground and ASIRAS are significantly different, yet the Pearson's correlation coefficient at t-43 are strongly positive. These results may be due to the small number of EGIG-Ground measurements (twelve) at t43.~~

5.3 ASIRAS-NP vs. ~~Polar MM5~~Regional Climate Models

Polar MM5 underestimates accumulation relative to ASIRAS-NP and EGIG-Ground (~~Figure ??~~Fig. 4). Mean Polar MM5 accumulation from 1985 to 2004 along EGIG is 0.06~~m~~ m (17 %) lower than ASIRAS-NP measurements. The mean 0.06~~m~~ m difference falls within Polar MM5's standard deviation of accumulation along EGIG (0.025~~to 0.075~~ 0.075) (Burgess et al., 2010). ~~The~~ Polar MM5's consistent underestimate of ~~Polar MM5~~ accumulation relative to ASIRAS-NP and EGIG-Ground may be explained by the measurements used to tune Polar MM5. Burgess et al. (2010) added spatial and temporal resolution to Greenland ice sheet accumulation by calibrating the Polar MM5 using firn cores and meteorological stations data. Burgess et al. (2010) re-sample the Polar MM5's 24 km horizontal grid output to a 1.25 km equal-area grid using bilinear interpolation (Burgess et al., 2010; Rignot et al., 2008). The 24 km original spacing results in approximately eight Polar MM5 data points along the 250 km EGIG line. These eight Polar MM5 points were tuned from a network of cores and automatic weather stations and thus were not forced to correspond exactly with cores along EGIG. Burgess et al. (2010) omit the majority of the ~~t-site~~ T-site accumulation rates along EGIG, including only sites ~~t31, t41, and t43~~T31, T41, and T43. ASIRAS-NP provides detailed accumulation measurements every ~~3m~~3 m, nearly continuous tracking along EGIG relative to Polar MM5. The increased ~~detail~~ spatial resolution may contribute to the ~~majority of the~~ difference in accumulation rates.

Yearly comparisons of the entire record of ASIRAS-NP and Polar MM5 snow accumulations (~~Figure ??~~Fig. 3) show positive correlations for ~~t21a, t23, t27, t41, t43 (Appendix Table~~**??**T21a, T23, T27, T41, T43 (Table **??**). Correlations between ASIRAS-NP and Polar MM5 demonstrate the model's utility for predicting the relative year-to-year accumulation trend. ASIRAS-NP and Polar MM5 both track the general ~~accumulation trend of higher accumulation near the coast decreasing to lower interior~~

accumulation rates coast to interior accumulation gradient as elevation increases (Figure ??). The observed accumulation gradient experiences aFig. 4). Morris and Wingham (2011) describe a noticeable change in surface conditions near site t-31 (Morris and Wingham, 2011) . T31 .

Above T31with undisturbed summer surface hoar from less persistent winds

Down-slope from t31 T31 katabatic winds pack the upper snow layer and form sastrugi, which may influence spatial variability and preservation of accumulation layers. Signal preserved in the upper ASIRAS-NP accumulation layers would be absent in the Polar MM5 record, possibly explaining Polar MM5's 2825 % accumulation underestimate compared to ASIRAS-NP below t-31T31. Elevations upslope from t31 T31 experience less persistent winds, leaving a smooth surface with undisturbed summer surface hoar, with a mean Polar MM5 accumulation 2418 % lower than ASIRAS-NP. The spatial gradient has a noticeable temporal component when comparing ASIRAS-NP and Polar MM5. From 1985 to 1994, ASIRAS-NP Polar MM5 accumulation is 28higher than Polar MM5 on both sides of t-31 % lower below T31 and 21 % lower above T31 compared to ASIRAS-NP. The east-west gradient along EGIG strengthens from 1995-2004, when ASIRAS-NP is 24higher than 1995 to 2004, when Polar MM5 below t-31 is 23 % lower than ASIRAS-NP below T31 and 16higher above t-31 % lower above T31. Polar MM5's recent accumulation rates near EGIG rely on firn cores drilled prior to 1995 and limited automatic weather stations at high elevation. Thus recent observed increases in accumulation at high elevation due to increased moisture availability from warming (de la Pena et al., 2010; Hawley et al., 2014) may not appear in the Polar MM5 record.

5.4 ASIRAS-NP vs. ASIRAS-HL: Accumulation Rate Sensitivity accumulation rate sensitivity to Densitydensity

Subtracting the ASIRAS-HL and ASIRAS-NP accumulation rates tests the radar-derived accumulation rate's sensitivity to density. The ASIRAS layers' position in radar time remains constant between the ASIRAS-NP and ASIRAS-HL. Density, which determines radar velocity and therefore water-equivalent depth, is the lone variable between ASIRAS-NP and ASIRAS-HL accumulation records. The largest differences in accumulation occur where NP and HL densities differ most. NP density profiles provide detailed vertical resolution of seasonal density fluctuation. Seasonal density fluctuations are most prominent in the near surface layers and in areas with large variability in temperature and accumulation (*e.g.* e.g. coastal, lower elevations). Though the simple three parameter Herron and Langway (1980) model cannot capture the detailed seasonal density variations, the model's general trend generalized density in the near-surface generates ASIRAS-HL accumulation rates within 4.5 % of ASIRAS-NP. NP and HL densities resemble each other most at deeper depths as compaction smooths seasonal fluctuations in density. Thus the deeper layers have the smallest mean percentage accumulation difference (3) (Figure %) (Fig. 5). The low (4.5 %) mean accumulation differences along EGIG indicate that modeled density values provide reasonable accumulation estimates in areas with low variability in density and where detailed density profiles are unavailable. Differences in accumulation decrease with increasing depth/age of the layers, as the HL model densities approach NP densities. Below 11 m depth, differences are related to Summit GISP2b-Shifted and Summit GISP2b shallow density core bounding the west (0 km) and east (250 km) margins, respectively, of the EGIG line. No dominant spatial pattern of accumulation differences emerges from west to east. The mean of the lower five accumulation years (1985 to 19891985–1989) account for the smallest accumulation differences from 60 to 250 km. The largest differences along EGIG occur on the east end (225 to

250 225–250 km) where ASIRAS-NP is constrained by a Summit density core. Abrupt jumps in mean percent accumulation difference occur where the number of layers included in the average change.

Recall the spatially continuous nature of the density inputs for the ASIRAS-HL accumulation record (74038 unique HL density profiles spaced 3 3 m apart). These density inputs were driven by highly resolved HL model inputs of accumulation, temperature and surface density. ASIRAS-HL accumulation accuracy relative to ASIRAS-NP may be due to these model inputs. We test this possibility with the HL250km, HL125kmHL250 km, HL125 km, etc., accumulation records, which rely on a limited number of density profiles and interpolation. The moderate reduction from 7 to 4.5 % accumulation difference for HL250 km and HL125 km is likely due to the linear gradients (increasing accumulation downslope, decreasing elevation, increasing temperature) of the HL model input parameters along the 250 km EGIG segment. The two density profiles of HL125 km cover both the lower and upper range of the gradients. The interpolation between these two HL125 profiles contains contain the majority of density variation seen in the ASIRAS-NP, thus accounting for the 4 % mean accumulation difference between ASIRAS-HL125km ASIRAS-HL125 km and ASIRAS-NP. An average 3.2 % percent accumulation difference can be obtained using 5 HL profiles at 50 km spacing. This finding stands to improve accuracy for radar-derived accumulation rates and serve as a guideline for correcting the wealth of IceBridge radar data.

6 Conclusions

6 Conclusions

Point-based measurements such as ice cores and weather stations provide the basis for current accumulation estimates. Models and interpolation between these points provide spatially continuous estimates of accumulation. Radar-detected annual accumulation layers offer a physical observation connecting point-based measurements. Detailed NP density measurements provide accurate radar travel-time velocities and exact densities for water-equivalent conversion, improving accuracy of annual accumulation rates from ASIRAS. We report spatially continuous annual accumulation rates from 1959 to 2004 along a 250 km segment of EGIG. Our ASIRAS-NP rates are not statistically different from EGIG-Ground point measurements spanning 1985-2004. Mean ASIRAS-NP accumulation along EGIG is 23higher than the mean 1985–2004. Polar MM5 model estimate. An east to west accumulation gradient along the EGIG line strengthens from 1995-2004, when and RACMO2.3 consistently underestimate accumulation by 17 % along EGIG compared to ASIRAS-NPis 35higher than . MAR underestimates by as much as 16 % and overestimates by 10 %. Overall, Regional Climate Models Polar MM5downslope from t-31 and 23higher upslope from t-31, MAR, and RACMO2.3 succeed in capturing the general trend of accumulation seen by ASIRAS-NP, but they underestimate the total amount of snow. The ASIRAS-NP observed increases in mean accumulation may relate to increased warming and availability of moisture at higher elevations.

The similarity between ASIRAS and EGIG-Ground demonstrates that the ASIRAS layers, adjusted with NP density, produce accurate estimates of accumulation along acontinuous 250km continuous 250 km segment of the EGIG line. We acknowledge recognize the challenge of obtaining detailed density measurements and demonstrate the use of simple HL models to derive adequate accumulation estimates. Using Herron and Langway (1980) profiles at 50 km intervals produces ASIRAS-

HL accumulation rates within 3 % of ASIRAS-NP estimates. High resolution airborne radar systems operated in dry snow regions of ice sheets, such as those onboard Operation IceBridge, calibrated with a minimal number of Herron and Langway (1980) modeled density profiles, may produce accumulation rates within the uncertainty of accumulation best-estimates using detailed density profiles.

Acknowledgements. This work was supported by the European Space Agency (ESA) as a part of the CryoSat program and by National Aeronautics and Space Administration (NASA) Grants NNX10AP04G and NNX10AG22G. The work of Veit Helm was funded by the German Federal Ministry of Economics and Technology (Grant 50EE1331). We thank all team members involved in the CryoVex 2006 campaign. We are especially grateful to the in situ calibration and validation team for their efforts collecting detailed neutron-probe data. We thank reviews Laura Koenig, Ginny Catania, two anonymous reviewers, and editor Marco Tedesco for their comments and handling of the manuscript.

References

Anklin, M. and Stauffer, B.: Pattern of annual snow accumulation along a west Greenland flow lone: no significant change observed during recent decades, Tellus B, 46, 294–303, 1994.

~~Appendix~~

Arcone, S., Spikes, V., Hamilton, G., and Mayewski, P. A.: Stratigraphic continuity in 400 MHz short-pulse radar profiles of firn in West Antarctica, Ann. Glaciol., 39, 195–200, 2004.

Arcone, S., Spikes, V., and Hamilton, G.: Stratigraphic variation within polar firn caused by differential accumulation and ice flow: interpretation of a 400 MHz short-pulse radar profile from West Antarctica, J. Glaciol., 51, 407–422, 2005.

~~Mean annual ASIRAS-NP accumulation () at t-sites along EGIG.~~

Bales, R. C., McConnell, J. R., Mosley-Thompson, E., and Csatho, B.: Accumulation over the Greenland ice sheet from historical and recent records, J. Geophys. Res.-Atmos., 106, 33813–33825, 2001.

Bales, R. C., Guo, Q., Shen, D., McConnell, J., Du, G., Burkhart, J. F., Spikes, V., Hanna, E., and Cappelen, J.: Annual accumulation for Greenland updated using ice core data developed during 2000–2006 and analysis of daily coastal meteorological data, J. Geophys. Res., 114, D06116, doi:10.1029/2008JD011208, 2009.

Banta, J. and McConnell, J. R.: Annual accumulation over recent centuries at four sites in central Greenland, J. Geophys. Res., 112, D10114, doi:10.1029/2006JD007887, 2007.

Benson, C.: Stratigraphic studies in the snow and firn of the Greenland ice sheet., Research Report 70, U.S. Army Snow, Ice and Permafrost Research Establishment, Corps of Engineers, 1962.

Black, H. and Budd, W.: Accumulation in the region of Wilkes, Wilkes Land, Antarctica, J. Glaciol., 5, 3–15, 1964.

Box, J. E., Bromwich, D. H., and Bai, L. S.: Greenland ice sheet surface mass balance 1991–2000: application of Polar MM5 mesoscale model and in situ data, J. Geophys. Res., 109, D16105, doi:10.1029/2003JD004451, 2004.

Bromwich, D. H., Chen, Q. S., Bai, L. S., Cassano, E., and Li, Y.: Modeled precipitation variability over the Greenland ice sheet, J. Geophys. Res., 106, 33891–33908, 2001.

Burgess, E., Forster, R. R., Box, J. E., Mosley-Thompson, E., Bromwich, D. H., Bales, R. C., and Smith, L.: A spatially calibrated model of annual accumulation rate on the Greenland Ice Sheet (1958–2007), J. Geophys. Res., 115, F02004, doi:10.1029/2009JF001293, 2010.

Cullen, R.: CryoVEx Airborne Data Products Description, ASIRAS 2.6.1, European Space Agency, ESTEC, Noordwijk, Netherlands, 2010.

Dansgaard, W.: Frozen Annals: Greenland Ice Sheet Research, Aage V. Jenkins Fonde (Denmark), 1st Edn., available at: http://www.nbi.ku.dk/english/www/willi/dansgaard/tilbage-til-groenland/, last access: 12 August 2015, 2004.

de la Peña, S., Nienow, P., Shepherd, A., Helm, V., Mair, D., Hanna, E., Huybrechts, P., Guo, Q., Cullen, R., and Wingham, D.: Spatially extensive estimates of annual accumulation in the dry snow zone of the Greenland Ice Sheet determined from radar altimetry, The Cryosphere, 4, 467–474, doi:10.5194/tc-4-467-2010, 2010.

Eisen, O., Frezzotti, M., Genthon, C., Isaksson, E., Magand, O., van den Broeke, M. R., Dixon, D., Ekaykin, A., Holmlund, P., Kameda, T., Karlöf, L., Kaspari, S., Lipenkov, V., Oerter, H., Takahashi, S., and Vaughan, D. G.: Ground-based measurements of spatial and temporal variability of snow accumulation in East Antarctica, Rev. Geophys., 46, RG2001, doi:10.1029/2006RG000218,2008.

Fischer, H., Wagenbach, D., Laternser, M., and Haeberli, W.: Glaciometerological and isotopic studies along the EGIG line, central Greenland ice sheet, J. Glaciol., 41, 515–527, 1995.

Hawley, R. L., Morris, E. M., Cullen, R., Nixdorf, U., Shepherd, A. P., and Wingham, D. J.: ASIRAS airborne radar resolves internal annual layers in the dry-snow zone of Greenland, Geophys. Res. Lett., 33, L04502, doi:10.1029/2005GL025147, 2006.

Hawley, R. L., Morris, E. M., and McConnell, J.: Intruments and methods rapid techniques for determining annual accumulation applied at Summit, Greenland, J. Glaciol., 54, 839–845, 2008.

Hawley, R. L., Courville, Z., Kehrl, L., Lutz, E., Osterberg, E., Overly, T., and Wong, G.: Recent accumulation variability in northwest Greenland from ground-penetrating radar and shallow cores along the Greenland Inland Traverse, J. Glaciol., 60, 375–382, 2014.

Helm, V., Rack, W., Cullen, R., Neinow, P., Mair, D., Parry, V., and Wingham, D. J.: Winter accumulation in the percolation zone of Greenland measured by airborne radar altimeter, Geophysical Research Letters, 34, doi:10.1029/2006GL029 185, 2007.

Herron, M. and Langway Jr., C.: Firn densification: an empirical model, J. Glaciol., 25, 373–385, 1980.

IPCC: Climate Change 2014 Synthesis Report, edited by: Pachauri, K., Meyer, L., and core writing team, Intergovernmental Panel on Climate Change, IPCC Secretariat, Geneva, Switzerland, 2014.

Kovacs, A., Gow, A. J., and Morey, R. M.: The in-situ dielectric constant of polar firn revisted, Cold Reg. Sci. Technol., 23, 245–256, 1995.

McConnell, J. R., Mosley-Thompson, E., Bromwich, D. H., Bales, R. C., and Kyne, J. D.: Interannual variations of snow accumulation on the Greenland Ice Sheet (1985-1996): new observations versus model predictions, J. Geophys. Res.-Atmos., 105, 4039–4046, 2000.

McConnell, J. R., Lamorey, G., Hanna, E., Mosley-Thompson, E., Bales, R. C., Belle-Oudry, D., and Kyne, J. D.: Annual net snow accumulation over southern Greenland from 1975 to 1998, J. Geophys. Res., 106, 33827–33837, 2001.

Medley, B., Joughin, I., Das, S., Steig, E. J., Conway, H., Gogineni, S., Criscitiello, A., McConnell, J., Smith, B., van den Broeke, M. R., Lenaerts, J., Bromwich, D., and Nicolas, J.: Airborne-radar and ice-core observations of annual snow accumulation over Thwaites Glacier, West Antarctica confirm the spatiotemporal variability of global and regional atmospheric models, Geophysical Research Letters, 40, 3649–3654, 2013.

Medley, B., Joughin, I., Smith, B., Das, S., Steig, E. J., Conway, H., Gogineni, S., Lewis, C., Criscitiello, A., McConnell, J. R., van den Broeke, M. R., Lenaerts, J., Bromwich, D., Nicolas, J., and Leuschen, C.: Constraining the recent mass balance of Pine Island and Thwaites glaciers, West Antarctica, with airborne observations of snow accumulation, The Cryosphere, 8, 1375–1392, 2014.

Merlivat, L., Lorius, C., Ravoire, J., and Vergnaud, J.: Tritium and deuterium content of the snow in Groenland, Earth and Planetary Science Letters, 19, 235–240, 1973.

Miége, C., Forster, R. R., Box, J. E., Burgess, E. W., McConnell, J. R., Pasteris, D. R., and Spikes, V. B.: Southeast Greenland high accumulation rates derived from firn cores and ground-penetrating radar, Ann. Glaciol., 54, 322–332, 2013.

Morris, E. M.: A theoretical analysis of the neutron-scattering method for measuring snow and ice density, J. Geophys. Res., 113, F03019, doi:10.1029/2007JF000962, 2008.

Morris, E. M. and Cooper, J.: Density measurements in ice boreholes using neutron scattering, J. Glaciol., 49, 599–604, 2003.

Morris, E. M. and Wingham, D. J.: The effect of fluctuations in surface density, accumulation and compaction on elevation change rates along the EGIG line, central Greenland, J. Glaciol., 57, 416–430, 2011.

Morris, E. M. and Wingham, D. J.: Densification of polar snow: measurements, modeling, and implications for altimetry, J. Geophys. Res.-Earth, 119, 349–365, 2014.

Table 1. Summary table of Mean Accumulation Rates, 1959–2004, for Fig. 4. Percentage change relative to previous 10-year period.

Period	ASIRAS-NP	MM5	MAR	RACMO
1959–2004	0.337 ± 0.03	0.288 ± 0.04	0.329 ± 0.03	0.279 ± 0.06
1995–2004	0.382 ± 0.03	0.307 ± 0.05	0.347 ± 0.02	0.306 ± 0.04
1984–1995	0.328 ± 0.02	0.279 ± 0.04	0.326 ± 0.02	0.279 ± 0.06
1975–1984	0.327 ± 0.01	0.299 ± 0.04	0.345 ± 0.03	0.283 ± 0.06
1965–1974	0.270 ± 0.01	0.272 ± 0.04	0.316 ± 0.03	0.257 ± 0.06
1959–1964	0.277 ± 0.01	0.276 ± 0.04	0.300 ± 0.02	0.263 ± 0.05

Mosley-Thompson, E., McConnell, J. R., Bales, R. C., Lin, P. N., Steffen, K., Thompson, L. G., Edwards, R., and Bathke, D.: Local to regional-scale variability of annual net accumulation on the Greenland ice sheet from PARCA cores, Journal Of Geophysical Research-Atmospheres, 106, 33 839–33 851, 2001.

Noël, B., van de Berg, W., van Meijgaard, E., Kuipers Munneke, P., van de Wal, R., and van den Broeke, M. R.: Evaluation of the updated regional climate model RACMO2.3: summer snowfall impact on the Greenland Ice Sheet, The Cryosphere, 9, 1831–1844, 2015.

NSIDC: GISP2 B-Core Density. The Greenland Summit Ice Cores CD-ROM, Tech. rep., National Snow and Ice Data Center, University of Colorado, Boulder, 1997.

Renaud, A., Schumacher, E., Hughes, B., Oeschger, H., and Mühlemann, C.: Tritium variations in Greenland Ice, Journal of Geophysical Research, 68, 3783, 1963.

Rignot, E., Box, J., and Burgess, E.: Mass balance of the Greenland ice sheet from 1958 to 2007, Geophys. Res. Lett., 35, L20502, doi:10.1029/2008GL035417, 2008.

Simonsen, S., Stenseng, S., A?algeirsdóttir, G., Fausto, R., Hvidberg, C. S., and Lucas-Picher, P.: Assessing a multilayered dynamic firn-compaction model for Greenland with ASIRAS radar measurements, Journal of Glaciology, 59, 545–558, 2013.

Spikes, V., Hamilton, G., Arcone, S., Kaspari, S., and Mayewski, P.: Variability in accumulation rates from GRP profiling on the West Antarctic plateau, Ann. Glaciol., 39, 238–244, 2004.

Steffen, K. and Box, J.: Surface climatology of the Greenland ice sheet: Greenland Climate Network 1995–1999, J. Geophys. Res., 106, 33951–33964, 2001.

Stenseng, L., Hvidegaard, S., Skourup, H., Forsberg, R., Andersen, C., Hanson, S., Cullen, R., and Helm, V.: Airborne Lidar and Radar Measurements In and Around Greenland CryoVEx 2006, Tech. rep., Danish National Space Institute, Copenhagen, Denmark, 2007.

Tedesco, M., Fettweis, X., and Alexander, P.: MAR v3.2 regional climate model data for Greenland (1958-2013). UCAR/NCAR - CISL - ACADIS., http://dx.doi.org/10.5065/D6JH3J7Z, 2015.

Wessel, P., W. H. F. Smith, R. Scharroo, J. F. Luis, and F. Wobbe, Generic Mapping Tools: Improved version released, EOS Trans. AGU, 94, 409-410, 2013.

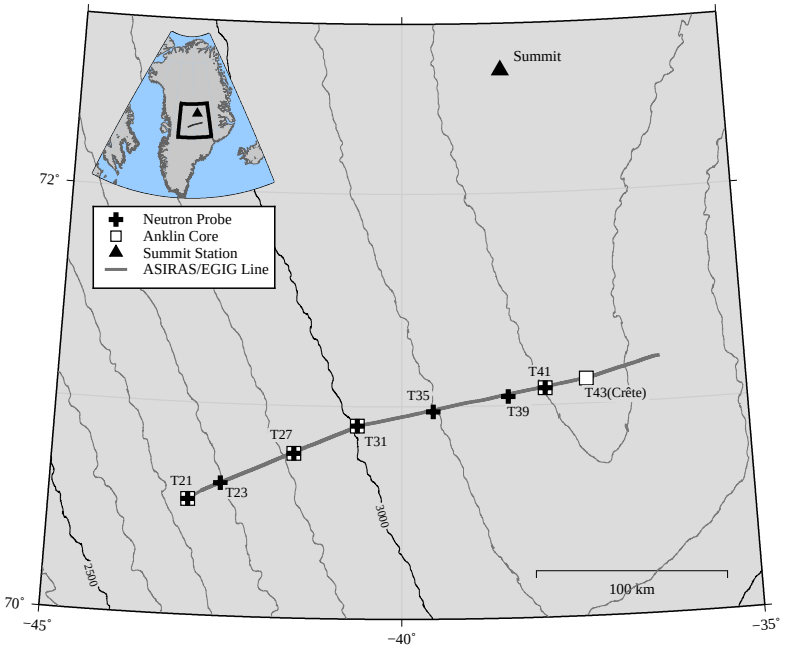

This work was supported by the European Space Agency (ESA) as a part of the CryoSat program and by National Aeronautics and Space Administration (NASA) Grants NNX10AP04G and NNX10AG22G. The work of Veit Helm was funded by the German Federal Ministry of Economics and Technology (Grant 50EE1331). We thank all team members involved in the CryoVex 2006 campaign. We are especially grateful to the in-situ calibration and validation team for their efforts collecting detailed Neutron Probe data. We thank the reviewers and editor Marco Tedesco for their comments and handling of the manuscript.

Summary table of Mean Accumulation Rates, 1985–2004, Summit Station for Figure ??reference. Percentage change relative to previous ten year period100 m contour intervals above 2000 m elevation are displayed. Scale bar accurate at 71° N latitude.

This work was supported by the European Space Agency (ESA) as a part of the CryoSat program and by National Aeronautics and Space Administration (NASA) Grants NNX10AP04G and NNX10AG22G. The work of Veit Helm was funded by the German Federal Ministry of Economics and Technology (Grant 50EE1331). We thank all team members involved in the CryoVex 2006 campaign. We are especially grateful to the in-situ calibration and validation team for their efforts collecting detailed Neutron Probe data. We thank the reviewers and editor Marco Tedesco for their comments and handling of the manuscript.

Summary table of Mean Accumulation Rates, 1985–2004, Summit Station for Figure ??reference. Percentage change relative to previous ten year period100 m contour intervals above 2000 m elevation are displayed. Scale bar accurate at 71° N latitude.

Figure 1. ASIRAS radargram Field locations along a portion of the forty-seven traced internal reflection horizons Expédition Glaciologique Internationale au Groenland (IRHsEGIG) , or layers, down to 30 depthtraverse. The uppermost layer represents the 2005 accumulation year. The deepest layer represent 1959. Distance along EGIG corresponds with t21 in Figure ??, with 0 250 km starting at 2700 segment of ASIRAS radar data discussed in this paper spans 2600 to 3200 m on elevation. Black crosses ✚ show neutron-probe density T-sites from Morris and Wingham (2011) . White squares □ show Anklin and Stauffer (1994) shallow cores. The filled triangle ▲ shows the western slope and extending beyond 350where layer visibility decreases on the eastern slope location of the Greenland Ice Sheet.

This work was supported by the European Space Agency (ESA) as a part of the CryoSat program and by National Aeronautics and Space

Table 2. Summary table of Mean Accumulation Rates, 1985–2004, for Fig. 4.

Study	T21	T27	T31	T41
EGIG-Ground	0.488 ± 0.03	0.405 ± 0.02	0.385 ± 0.02	0.294 ± 0.01
ASIRAS	0.455 ± 0.02	0.409 ± 0.02	0.378 ± 0.01	0.297 ± 0.01
MM5	0.370 ± 0.01	0.333 ± 0.01	0.311 ± 0.06	0.257 ± 0.06
MAR	0.373 ± 0.02	0.357 ± 0.02	0.344 ± 0.01	0.322 ± 0.01
RACMO2.3	0.390 ± 0.02	0.348 ± 0.02	0.318 ± 0.01	0.233 ± 0.01

– continued from previous page

Table 3. Mean percentage difference between ASIRAS-NP and RCMs for periods 1985–1994, 1995–2004, 1985–2004

Period	RACMO	MAR	MM5
	EGIG		
1985–2004	18 %	3 %	17 %
1995–2004	17 %	4 %	13 %
1985–1994	13 %	-4 %	21 %
	Below T31		
1985–2004	16 %	16 %	20 %
1995–2004	17 %	17 %	16 %
1985–1994	9 %	8 %	25 %
	Above T31		
1985–2004	18 %	-4 %	15 %
1995–2004	17 %	-3 %	12 %
1985–1994	16 %	-10 %	19 %

Table A1. Mean annual ASIRAS-NP accumulation (m w.e.) at T-sites along EGIG.

Year	T21	T21a	T23	T27	T31	T35	T39	T41
Lat	70.54	70.59	70.62	70.78	70.91	70.98	71.04	71.08
Lon	-43.03 –43.03	-42.79 –42.79	-42.58 –42.58	-41.54 –41.54	-40.64 –40.64	-39.55 –39.55	-38.46 –38.46	-37.92 –37.
2004	0.64 0.64 ± 0.01	0.67 0.67 ± 0.01	0.64 0.64 ± 0.01	0.56 0.56 ± 0.01	0.49 0.49 ± 0.01	0.40 0.40 ± 0.01	0.36 0.36 ± 0.01	0.33 0.33 ± 0
2003	0.56 0.56 ± 0.01	0.58 0.58 ± 0.01	0.61 0.61 ± 0.01	0.48 0.48 ± 0.01	0.43 0.43 ± 0.01	0.37 0.37 ± 0.01	0.33 0.33 ± 0.01	0.30 0.30 ± 0
2002	0.39 0.39 ± 0.01	0.41 0.41 ± 0.01	0.39 0.39 ± 0.01	0.38 0.38 ± 0.01	0.38 0.38 ± 0.01	0.34 0.34 ± 0.01	0.30 0.30 ± 0.01	0.32 0.32 ± 0
2001	0.56 0.56 ± 0.01	0.58 0.58 ± 0.01	0.48 0.48 ± 0.01	0.41 0.41 ± 0.01	0.36 0.36 ± 0.01	0.36 0.36 ± 0.01	0.32 0.32 ± 0.01	0.29 0.29 ± 0
2000	0.56 0.56 ± 0.01	0.54 0.54 ± 0.01	0.52 0.52 ± 0.01	0.42 0.42 ± 0.01	0.35 0.35 ± 0.01	0.28 0.28 ± 0.01	0.29 0.29 ± 0.01	0.25 0.25 ± 0
1999	0.49 0.49 ± 0.03	0.41 0.41 ± 0.03	0.52 0.52 ± 0.01	0.54 0.54 ± 0.01	0.47 0.47 ± 0.01	0.46 0.46 ± 0.01	0.39 0.39 ± 0.01	0.38 0.38 ± 0
1998	0.40 0.40 ± 0.01	0.42 0.42 ± 0.01	0.40 0.40 ± 0.01	0.31 0.31 ± 0.01	0.31 0.31 ± 0.01	0.25 0.25 ± 0.01	0.23 0.23 ± 0.01	0.24 0.24 ± 0
1997	0.45 0.45 ± 0.01	0.44 0.44 ± 0.01	0.46 0.46 ± 0.01	0.42 0.42 ± 0.01	0.39 0.39 ± 0.02	0.33 0.33 ± 0.01	0.31 0.31 ± 0.01	0.29 0.29 ± 0
1996	0.50 0.50 ± 0.01	0.51 0.51 ± 0.01	0.50 0.50 ± 0.01	0.46 0.46 ± 0.01	0.47 0.47 ± 0.04	0.47 0.47 ± 0.01	0.44 0.44 ± 0.01	0.39 0.39 ± 0
1995	0.61 0.61 ± 0.02	0.55 0.55 ± 0.02	0.59 0.59 ± 0.01	0.53 0.53 ± 0.02	0.43 0.43 ± 0.03	0.41 0.41 ± 0.01	0.34 0.34 ± 0.01	0.33 0.33 ± 0
1994	0.34 0.34 ± 0.01	0.32 0.32 ± 0.01	0.35 0.35 ± 0.01	0.34 0.34 ± 0.01	0.32 0.32 ± 0.01	0.26 0.26 ± 0.01	0.26 0.26 ± 0.01	0.25 0.25 ± 0
1993	0.36 0.36 ± 0.01	0.36 0.36 ± 0.01	0.34 0.34 ± 0.01	0.28 0.28 ± 0.01	0.27 0.27 ± 0.01	0.23 0.23 ± 0.01	0.23 0.23 ± 0.01	0.23 0.23 ± 0
1992	0.29 0.29 ± 0.01	0.33 0.33 ± 0.01	0.32 0.32 ± 0.01	0.30 0.30 ± 0.01	0.29 0.29 ± 0.01	0.29 0.29 ± 0.01	0.29 0.29 ± 0.01	0.26 0.26 ± 0
1991	0.58 0.58 ± 0.01	0.53 0.53 ± 0.01	0.50 0.50 ± 0.03	0.40 0.40 ± 0.01	0.39 0.39 ± 0.02	0.39 0.39 ± 0.01	0.34 0.34 ± 0.01	0.35 0.35 ± 0
1990	0.44 0.44 ± 0.01	0.46 0.46 ± 0.01	0.49 0.49 ± 0.02	0.46 0.46 ± 0.01	0.42 0.42 ± 0.02	0.39 0.39 ± 0.01	0.36 0.36 ± 0.01	0.34 0.34 ± 0
1989	0.40 0.40 ± 0.01	0.40 0.40 ± 0.01	0.41 0.41 ± 0.01	0.40 0.40 ± 0.01	0.38 0.38 ± 0.01	0.30 0.30 ± 0.01	0.30 0.30 ± 0.01	0.28 0.28 ± 0
1988	0.40 0.40 ± 0.01	0.40 0.40 ± 0.01	0.41 0.41 ± 0.01	0.34 0.34 ± 0.01	0.30 0.30 ± 0.01	0.26 0.26 ± 0.01	0.27 0.27 ± 0.01	0.24 0.24 ± 0
1987	0.39 0.39 ± 0.01	0.39 0.39 ± 0.01	0.38 0.38 ± 0.01	0.33 0.33 ± 0.02	0.34 0.34 ± 0.01	0.33 0.33 ± 0.01	0.28 0.28 ± 0.01	0.28 0.28 ± 0
1986	–	–	0.33 0.33 ± 0.05	0.43 0.43 ± 0.02	0.40 0.40 ± 0.01	0.34 0.34 ± 0.01	0.32 0.32 ± 0.01	0.34 0.34 ± 0
1985	–	–	0.66 0.66 ± 0.08	0.49 0.49 ± 0.02	0.44 0.44 ± 0.01	0.43 0.43 ± 0.01	0.31 0.31 ± 0.01	0.26 0.26 ± 0
1984	–	–	0.47 0.47 ± 0.01	0.42 0.42 ± 0.04	0.32 0.32 ± 0.01	0.26 0.26 ± 0.02	0.27 0.27 ± 0.01	0.27 0.27 ± 0
1983	–	–	0.47 0.47 ± 0.01	0.51 0.51 ± 0.01	0.48 0.48 ± 0.02	0.35 0.35 ± 0.01	0.34 0.34 ± 0.01	0.35 0.35 ± 0
1982	–	–	0.32 0.32 ± 0.01	0.29 0.29 ± 0.03	0.27 0.27 ± 0.02	0.27 0.27 ± 0.01	0.28 0.28 ± 0.01	0.25 0.25 ± 0
1981	–	–	0.41 0.41 ± 0.01	0.33 0.33 ± 0.02	0.29 0.29 ± 0.02	0.27 0.27 ± 0.01	0.21 0.21 ± 0.02	0.22 0.22 ± 0
1980	–	–	0.27 0.27 ± 0.01	0.38 0.38 ± 0.02	0.33 0.33 ± 0.01	0.29 0.29 ± 0.01	0.29 0.29 ± 0.02	0.26 0.26 ± 0
1979	–	–	0.32 0.32 ± 0.01	0.23 0.23 ± 0.02	0.29 0.29 ± 0.01	0.26 0.26 ± 0.01	0.28 0.28 ± 0.02	0.26 0.26 ± 0

Table A1. Continued.

Year	T21	T21a	T23	T27	T31	T35	T39	T41	T43
Lat	70.54	70.59	70.62	70.78	70.91	70.98	71.04	71.08	71.12
Lon	−43.03	−42.79	−42.58	−41.54	−40.64	−39.55	−38.46	−37.92	−37.3
1978	–	–	0.46 0.46 ± 0.01	0.43 0.43 ± 0.01	0.35 0.35 ± 0.01	0.34 0.34 ± 0.01	0.28 0.28 ± 0.01	0.28 0.28 ± 0.01	0.240.24 ±
1977	–	–	0.57 0.57 ± 0.01	0.51 0.51 ± 0.01	0.38 0.38 ± 0.01	0.35 0.35 ± 0.01	0.34 0.34 ± 0.01	0.27 0.27 ± 0.02	0.280.28 ±
1976	–	–	0.40 0.40 ± 0.01	0.39 0.39 ± 0.01	0.38 0.38 ± 0.01	0.37 0.37 ± 0.01	0.28 0.28 ± 0.02	0.31 0.31 ± 0.01	0.240.24 ±
1975	–	–	0.42 0.42 ± 0.01	0.54 0.54 ± 0.01	0.42 0.42 ± 0.02	0.27 0.27 ± 0.02	0.30 0.30 ± 0.01	0.31 0.31 ± 0.01	0.340.34 ±
1974	–	–	0.31 0.31 ± 0.01	0.30 0.30 ± 0.01	0.43 0.43 ± 0.01	0.37 0.37 ± 0.01	0.34 0.34 ± 0.01	0.28 0.28 ± 0.01	0.250.25 ±
1973	–	–	0.33 0.33 ± 0.01	0.31 0.31 ± 0.01	0.29 0.29 ± 0.01	0.26 0.26 ± 0.01	0.24 0.24 ± 0.01	0.23 0.23 ± 0.01	0.260.26 ±
1972	–	–	–	–	0.32 0.32 ± 0.02	0.33 0.33 ± 0.02	0.28 0.28 ± 0.01	0.31 0.31 ± 0.01	0.310.31 ±
1971	–	–	–	–	0.32 0.32 ± 0.01	0.31 0.31 ± 0.01	0.26 0.26 ± 0.01	0.25 0.25 ± 0.01	0.250.25 ±
1970	–	–	–	–	0.28 0.28 ± 0.01	0.28 0.28 ± 0.01	0.28 0.28 ± 0.01	0.27 0.27 ± 0.01	0.250.25 ±
1969	–	–	–	–	0.41 0.41 ± 0.01	0.32 0.32 ± 0.01	0.23 0.23 ± 0.01	0.24 0.24 ± 0.01	0.220.22 ±
1968	–	–	–	–	0.30 0.30 ± 0.01	0.28 0.28 ± 0.01	0.28 0.28 ± 0.01	0.26 0.26 ± 0.01	0.250.25 ±
1967	–	–	–	–	0.29 0.29 ± 0.01	0.28 0.28 ± 0.01	0.28 0.28 ± 0.01	0.28 0.28 ± 0.01	0.260.26 ±
1966	–	–	–	–	0.27 0.27 ± 0.01	0.31 0.31 ± 0.02	0.22 0.22 ± 0.01	0.23 0.23 ± 0.01	0.190.19 ±
1965	–	–	–	–	0.24 0.24 ± 0.01	0.22 0.22 ± 0.01	0.23 0.23 ± 0.01	0.22 0.22 ± 0.01	0.230.23 ±
1964	–	–	–	–	0.34 0.34 ± 0.01	0.35 0.35 ± 0.01	0.34 0.34 ± 0.01	0.34 0.34 ± 0.01	0.280.28 ±
1963	–	–	–	–	0.31 0.31 ± 0.01	0.31 0.31 ± 0.01	0.29 0.29 ± 0.01	0.29 0.29 ± 0.01	0.290.29 ±
1962	–	–	–	–	0.24 0.24 ± 0.01	0.24 0.24 ± 0.01	0.20 0.20 ± 0.01	0.23 0.23 ± 0.01	0.230.23 ±
1961	–	–	–	–	0.23 0.23 ± 0.01	0.24 0.24 ± 0.01	0.24 0.24 ± 0.01	0.25 0.25 ± 0.01	0.230.23 ±
1960	–	–	–	–	0.28 0.28 ± 0.01	0.28 0.28 ± 0.01	0.27 0.27 ± 0.01	0.27 0.27 ± 0.01	0.240.24 ±
1959	–	–	–	–	0.34 0.34 ± 0.01	0.35 0.35 ± 0.01	0.32 0.32 ± 0.01	0.33 0.33 ± 0.01	0.300.30 ±

Paired Wilcoxon Rank Sum comparison of

Table A2. Pearson's Correlation Coefficients for Accumulation Figure **??**Fig.The Wilcoxon signed rank test is a nonparametric test for two populations when the observations are paired 3. *p* is the probability of observing a test statistic as or more extreme than the observed value under the null hypothesisEGIG-Ground, ASIRAS-NP, RCMs .alternate hypothesis states that the data in x come from a continuous distribution with median different than 0. Tests the null hypothesis that data in the vector x come from a distribution whose median is zero at the 5significance level.

Paired
ASIRAS-NP and EGIG-Ground ASIRAS-
EGIG-Ground ASIRAS-NP and Polar MM5
Pearson's Correlation Coefficients for Accumulation Figure **??**. EGIG-Ground vs. ASIRAS and EGIG-Ground vs. Polar MM5 Paired t21 t27 t31 t4
ASIRAS-NP Polar MM5 and RACMO2.3

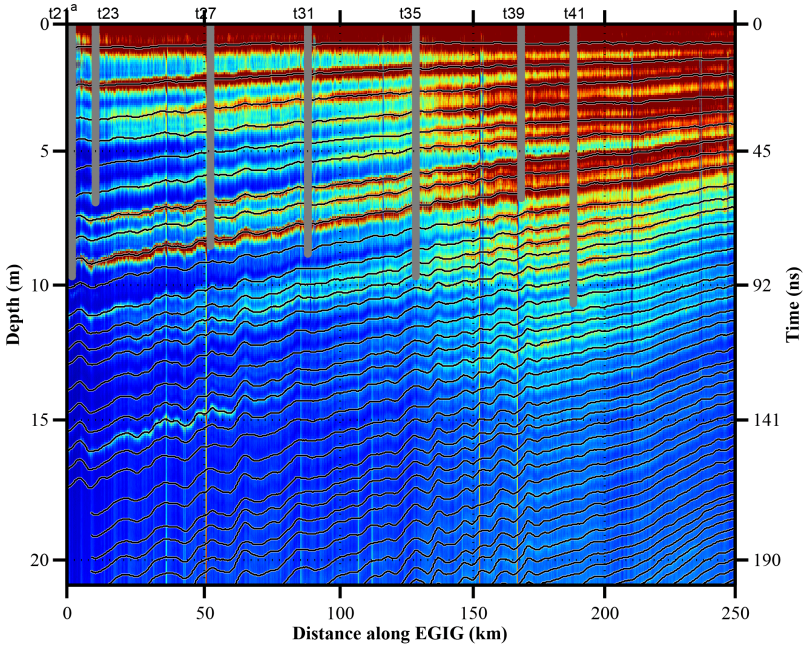

Figure 2. ASIRAS radargram of a portion of the forty-seven traced internal reflection horizons~~(IRHs)~~, or layers, down to ~~25~~ 20 m depth. The uppermost layer represents the 2005 accumulation year. ~~The deepest layer represent 1978.~~ Distance along EGIG corresponds with gray line in ~~Figure ??~~Fig. 6, with 0 km starting at 2700 m on the western slope and 250 km ending below 3200 m on the eastern slope of the Greenland Ice Sheet. ~~Near-surface layers appear down to 10 depth.~~ The left axis shows depth for NP and Internal Reflection Horizons. The right axis shows two-way travel time of an ASIRAS radar pulse. ~~High coastal accumulation rates, evident from thicker western layers from 0 to 50km, gradually thin with increasing elevation and orographic deposition of accumulation approaching the ice divide at 210 distance~~See Appendix Fig. ~~Topographic effects related to local surface features (described by Black and Budd (1964)) may explain layer undulations. Vertical gray lines indicate the position and depth~~ A1 for full extend of ~~Morris and Wingham (2011) NP density measurements.~~layers across EGIG

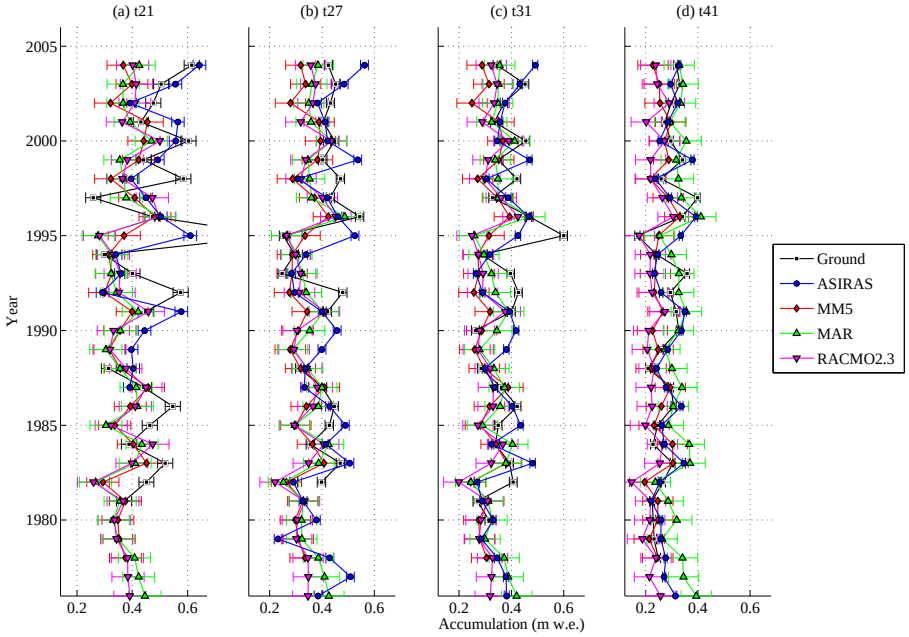

Figure 3. Mean annual accumulation rates at ~~t21~~T21, ~~t27~~T27, ~~t31~~T31, ~~t41,~~ and ~~t43,~~ T41 from ASIRAS-NP, RACMO2.3, MAR, Polar MM5 Model~~(Burgess et al., 2010)~~, and combined EGIG-Ground measurements from ~~Anklin and Stauffer (1994); Morris and Wingham (2011)~~ Anklin and Stauffer (1994) and Morris and Wingham (2011). ASIRAS-NP and EGIG-Ground accumulation rates from 1985 to 2004 are not statistically different at the four sites~~t21, t27, t31, and t41~~. ~~Polar MM5 accumulations are generally lower than ASIRAS accumulations but mostly remain within each other's uncertainty. Accumulation rate and fluctuation of~~ The RCMs underestimate accumulation ~~decreases from t21~~ compared to ~~t43 as site elevation increases and accumulation rates stabilize across~~ ASIRAS-NP, but succeed in tracking the ~~interior of the ice sheet. The~~ general ~~agreement of the three~~ accumulation ~~rates demonstrates ASIRAS's ability to track accumulation~~ trend across the 250 km EGIG ~~route~~segment.~~The lower panels display the mean accum rates. The EGIG-Ground mean is significantly different from Polar MM5 means at t21, t27, t31 for the entire record.~~

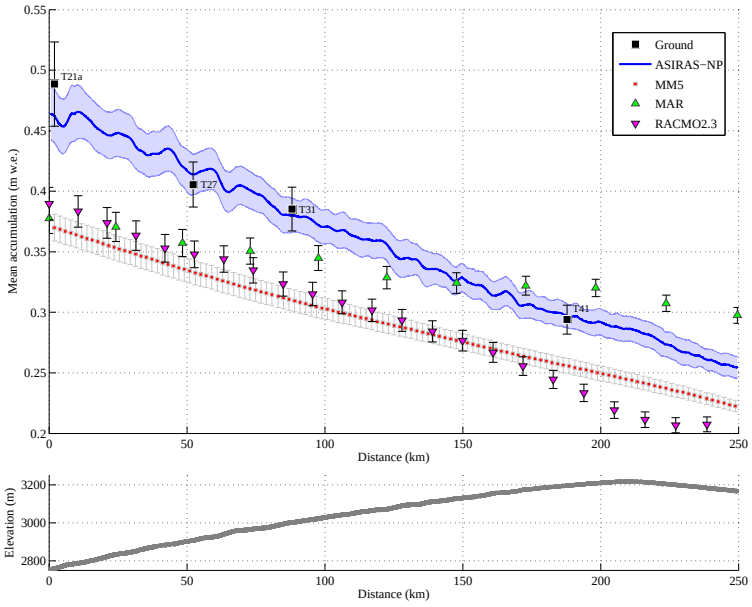

Figure 4. Mean water-equivalent accumulations rates from 1985 to 2004 along EGIG line. Solid dark blue line shows this study's ASIRAS-NP accumulation derived from ASIRAS layers and NP densities. Black squares depict mean accumulation from ~~t-sites~~ T-sites with NP/Core EGIG-Ground measurements from ~~Anklin and Stauffer (1994); Morris and Wingham (2011)~~ Anklin and Stauffer (1994) and Morris and Wingham (2011) spanning ~~1985 to 2004~~ 1985–2004 (~~T-21~~T21, ~~T-27~~T27, ~~T-31~~T31, ~~T-41~~T41). Snow accumulation from three Regional Climate Models, Polar MM5, MAR, and RACMO2.3 is plotted for comparison. The models generally underestimate accumulation compared to ~~ASIRAS~~ ASIRAS-NP and EGIG-Ground ~~in-situ~~ in situ estimates. Radar-derived accumulation rates are highest near the coast where density values have the largest range. Standard uncertainties displayed are for accumulation values from 1985 to 2004.

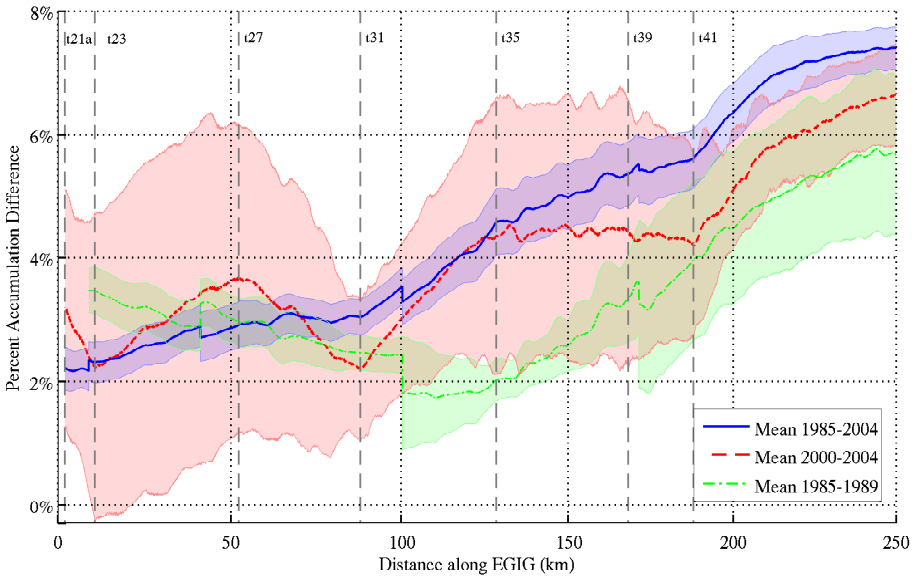

Figure 5. Mean percentage accumulation difference between ASIRAS-NP and ASIRAS-HL for the upper five (~~2000 to 2004~~2000–2004), lower five (~~1985-1989~~1985–1989), and ~~1985 to 2004~~ 1985–2004 layers. In general, differences in accumulation decrease with increasing depth/age of the layers. ASIRAS-HL accumulation differs from ASIRAS-NP accumulation by 4.5 % for the ~~1985 to 2004~~ 1985–2004 period. The low mean differences across the 250 km EGIG segment indicate that modeled densities provide accurate accumulation estimates in radar survey regions lacking ~~in-situ~~ in situ density measurements.

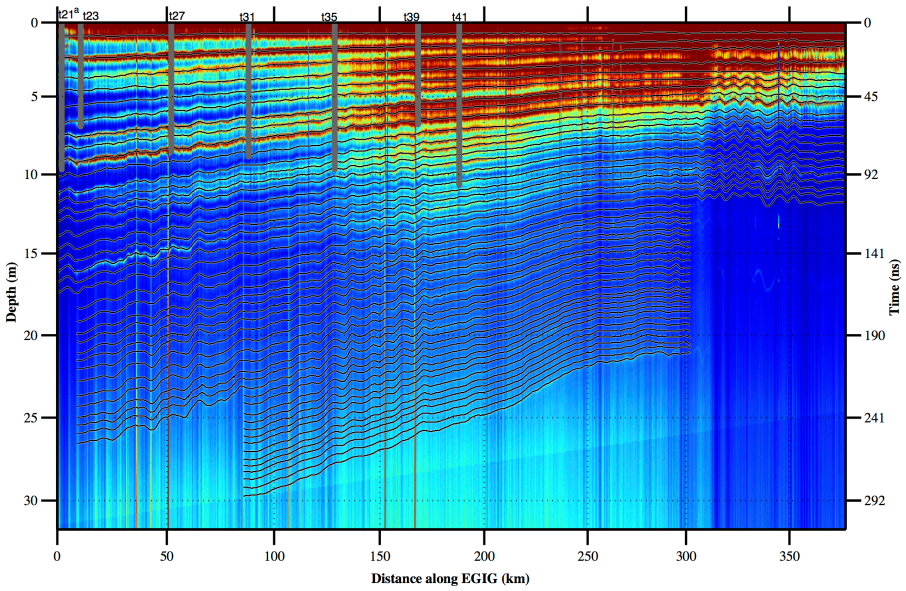

Figure A1. ASIRAS radargram of the forty-seven traced internal reflection horizons (IRHs), or layers, down to 30 m depth. The uppermost layer represents the 2005 accumulation year. The deepest layer represent 1959. Distance along EGIG corresponds with T21 in Fig. 6, with 0 km starting at 2700 m on the western slope and extending beyond 350 km where layer visibility decreases on the eastern slope of the Greenland Ice Sheet. High coastal accumulation rates, evident from thicker western layers from 0 to 50 km, gradually thin with increasing elevation and orographic deposition of accumulation approaching the ice divide at 210 m distance. Topographic effects related to local surface features (described by Black and Budd, 1964) may explain layer undulations. Vertical gray lines indicate the position and depth of Morris and Wingham (2011) NP density measurements.